Supporting Information:

Synthesis and Characterization of C_2 Symmetry Bis(Carboxamide) Pincer Ligands

Rufaro Razuwika[*,a] and Orde Q. Munro*[a,b]

[a] Molecular Sciences Institute, School of Chemistry, University of the Witwatersrand, PO WITS 2050, Johannesburg, South Africa

[b] School of Chemistry, University of Leeds, Woodhouse Road, Leeds, LS2 9JT, UK

Email: razuwika@gmail.com

Email: o.munro@leeds.ac.uk

Contents

IR instrumentation and spectra

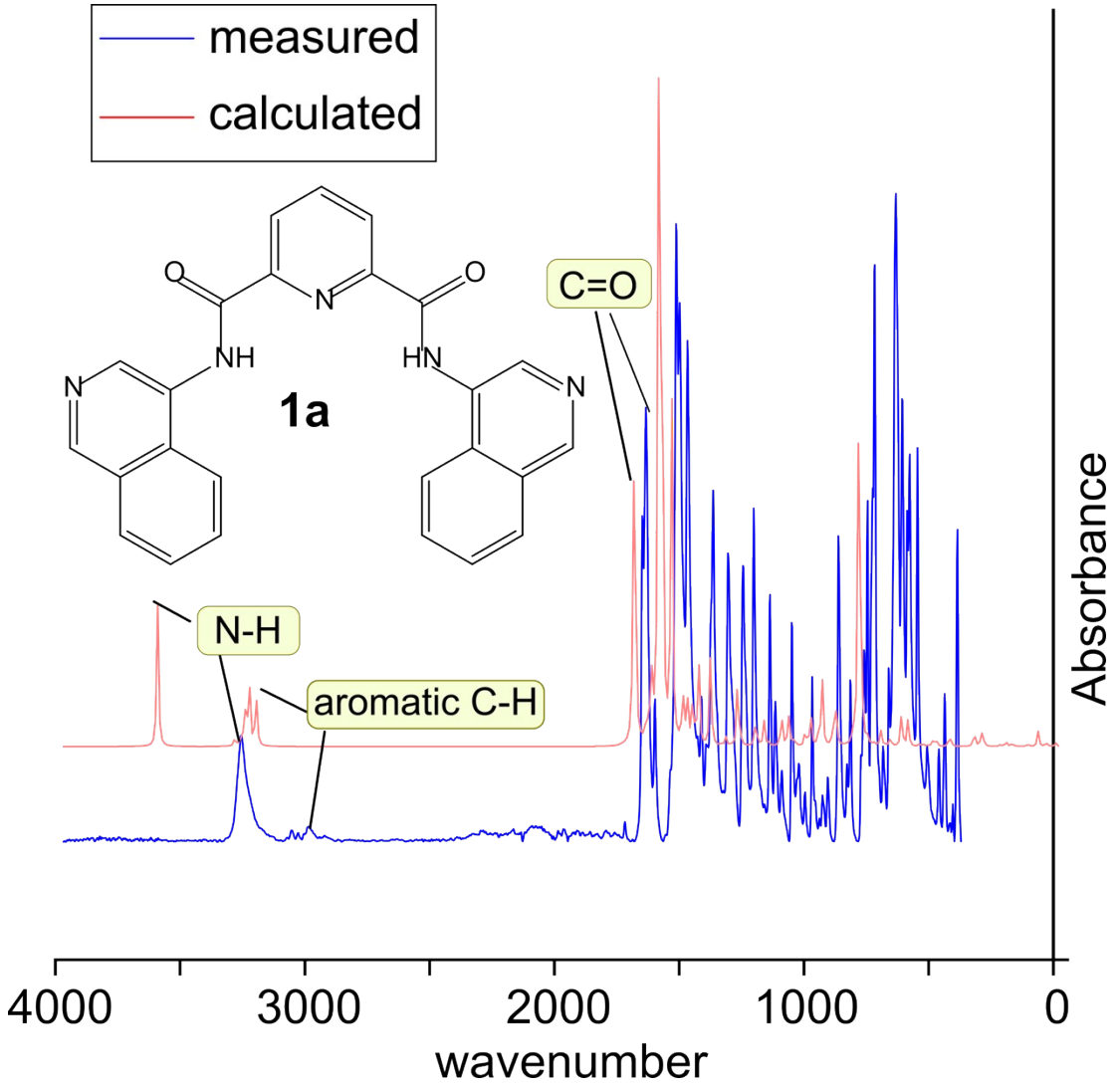

Figure S1. IR spectra for a powder sample (blue) and from DFT calculated data in a vacuum (red) of **1a**.

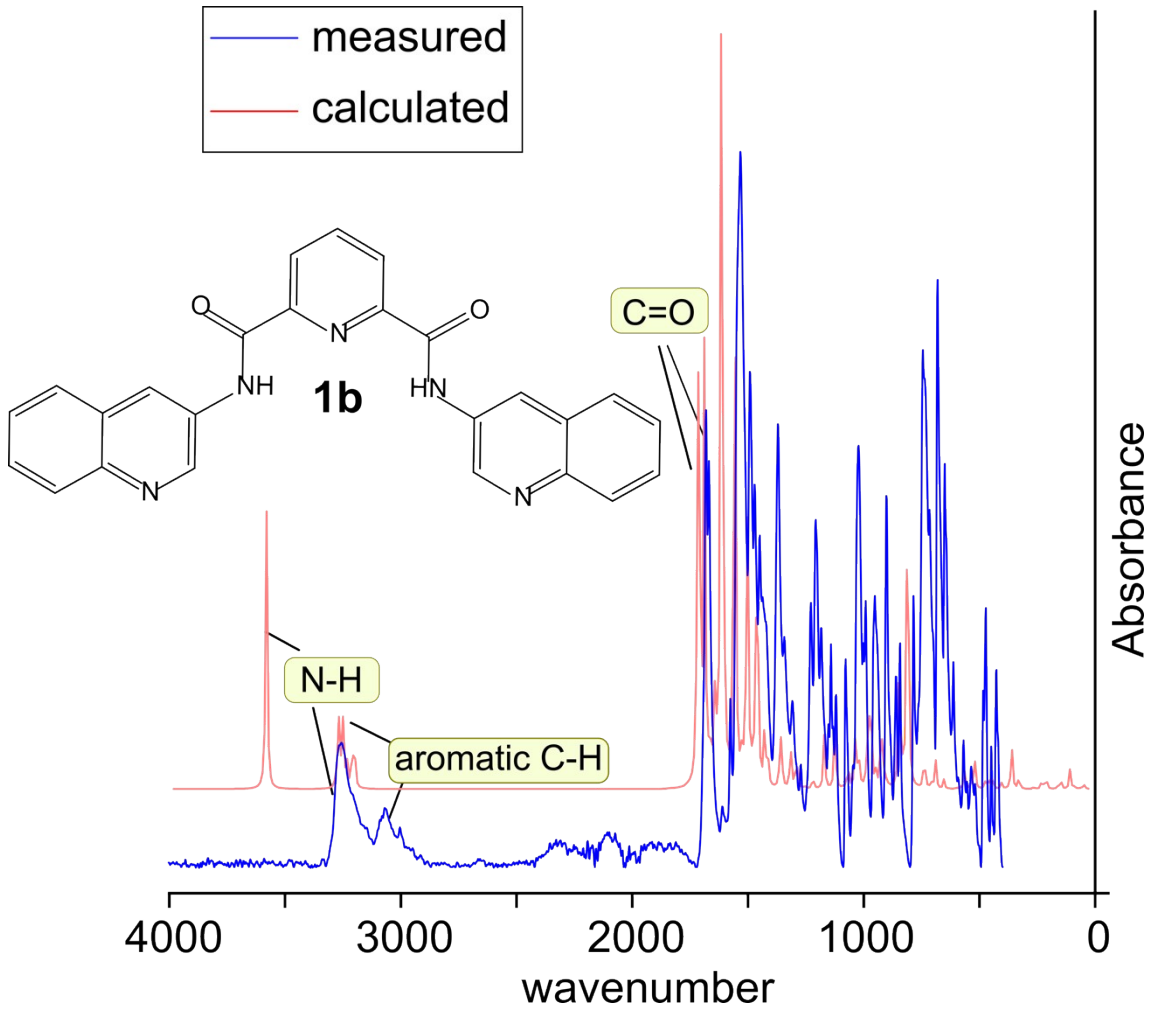

Figure S2. IR spectra for a powder sample (blue) and from DFT calculated data in a vacuum (red) of **1b**.

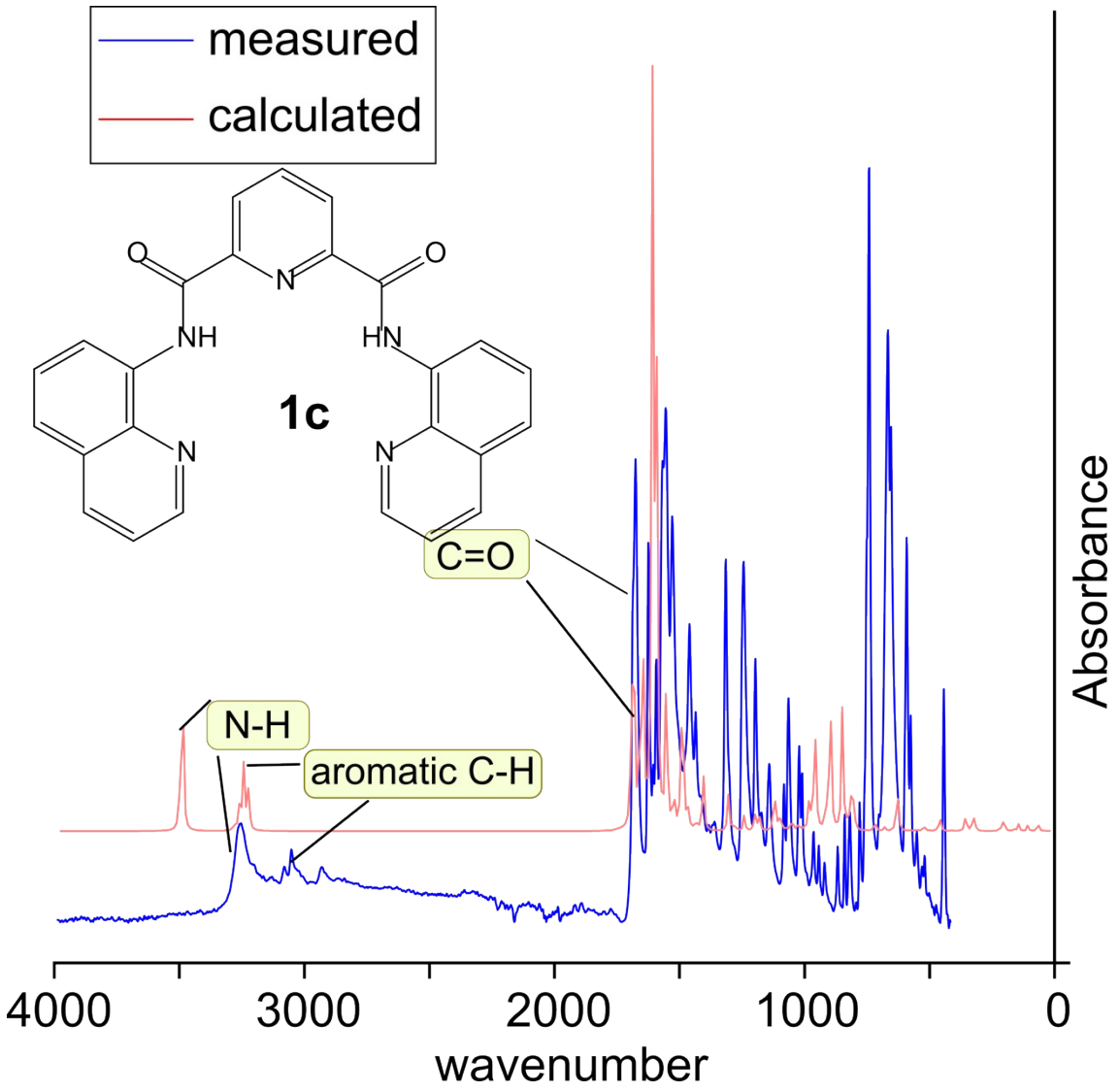

Figure S3. IR spectra for a powder sample (blue) and from DFT calculated data in a vacuum (red) of **1c**.

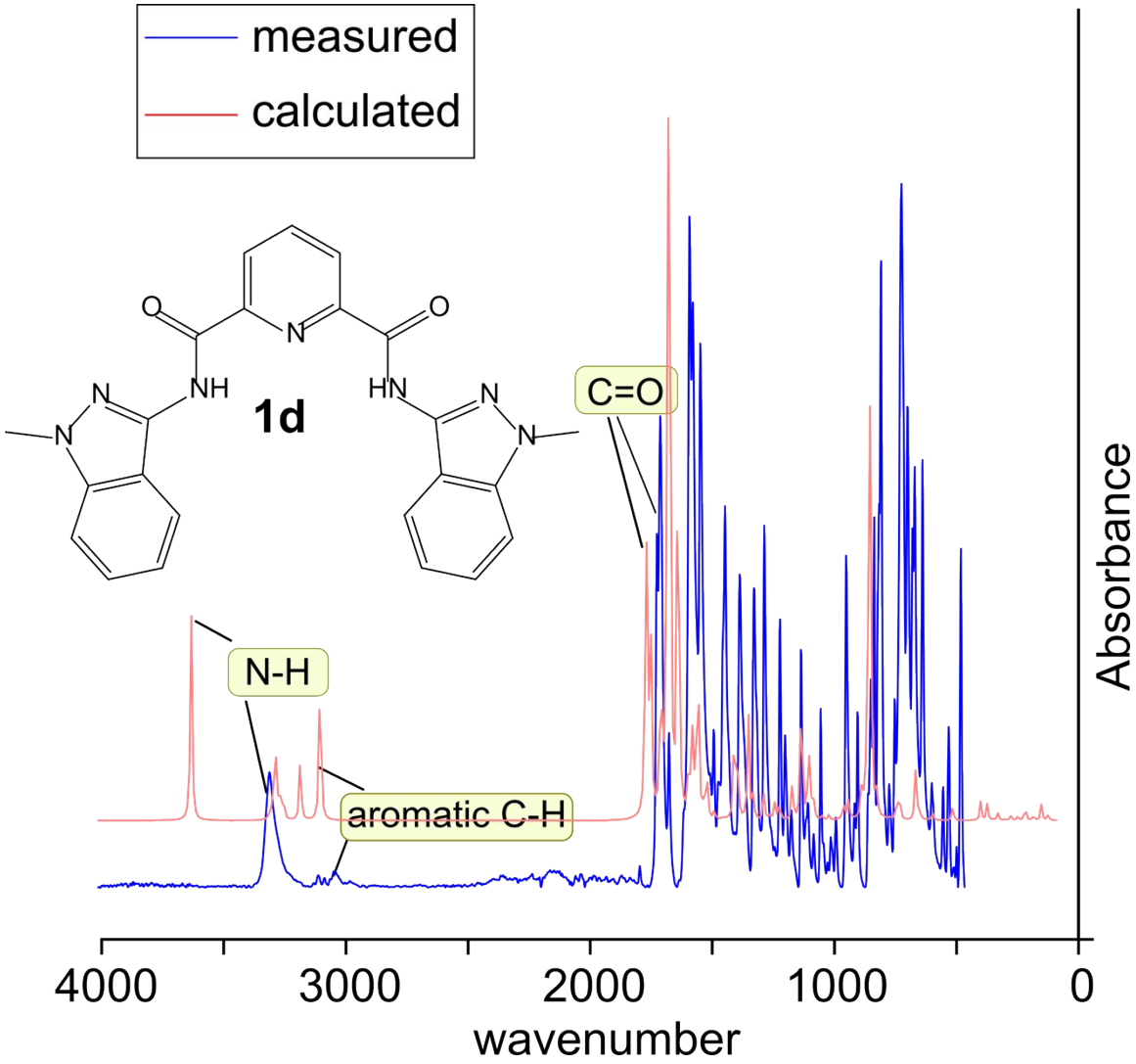

Figure S4. IR spectra for a powder sample (blue) and from DFT calculated data in a vacuum (red) of **1d**.

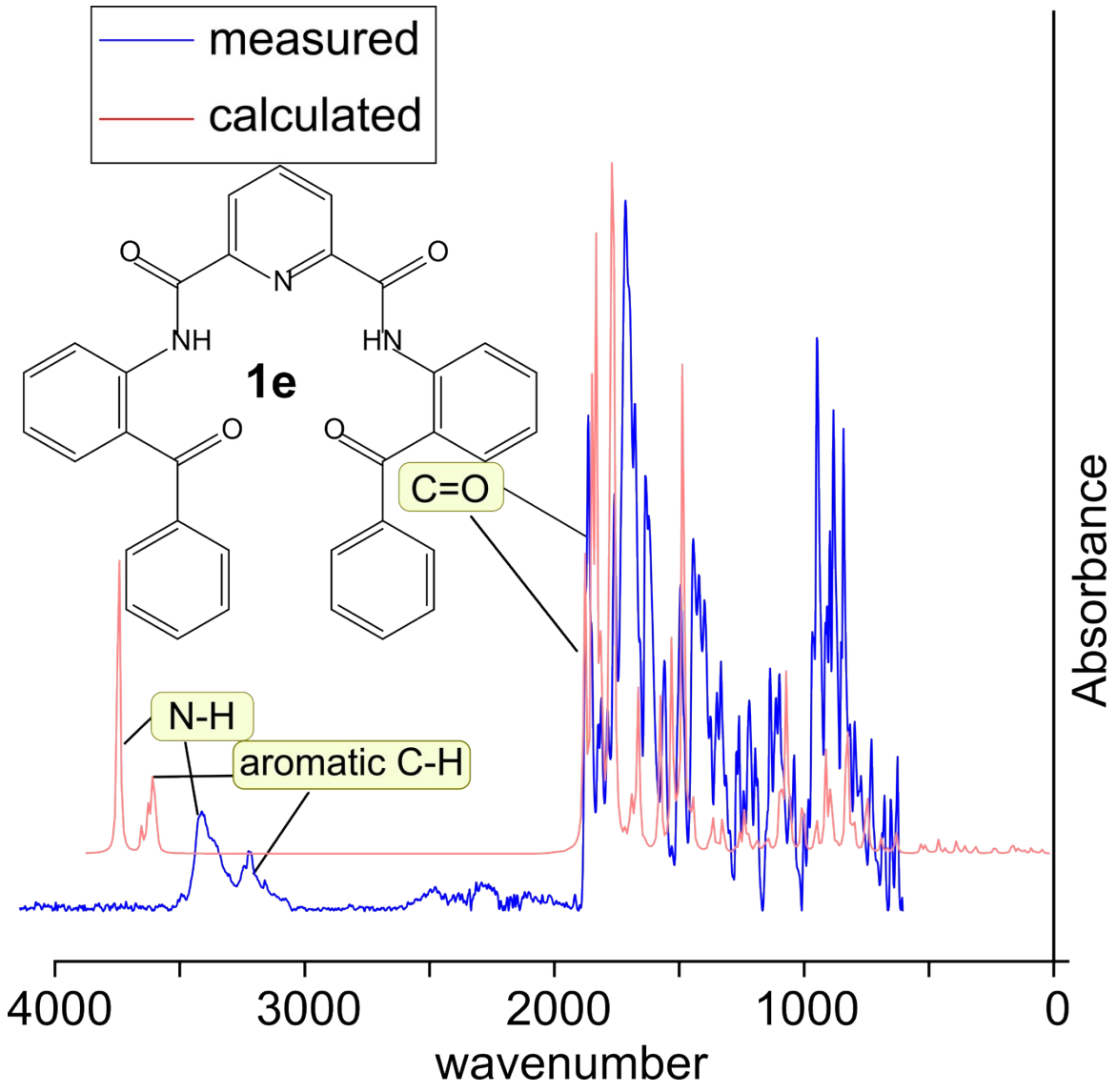

Figure S5. IR spectra for a powder sample (blue) and from DFT calculated data in a vacuum (red) of **1e.**

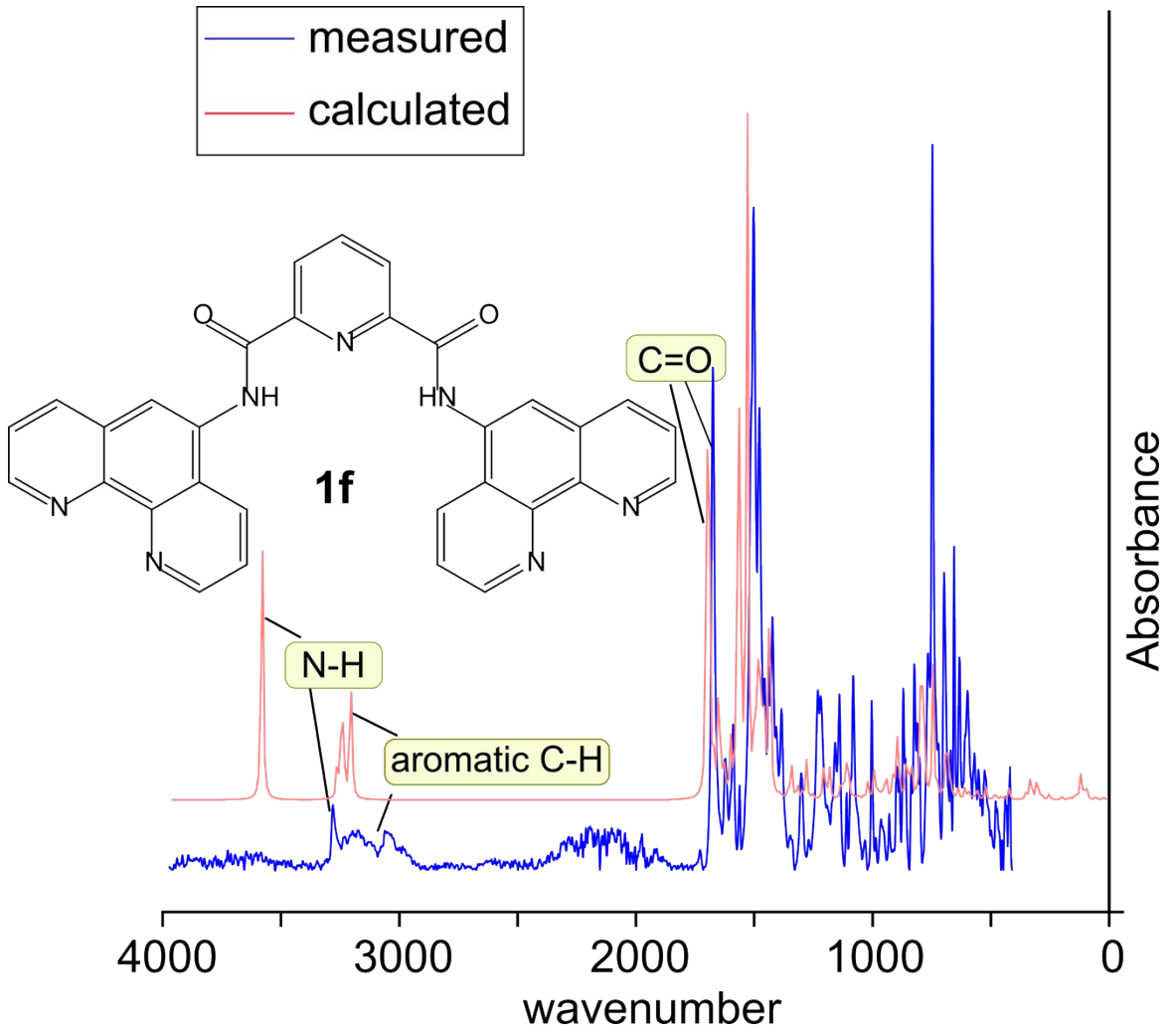

Figure S6. IR spectra for a powder sample (blue) and from DFT calculated data in a vacuum (red) of **1f**.

NMR spectroscopy

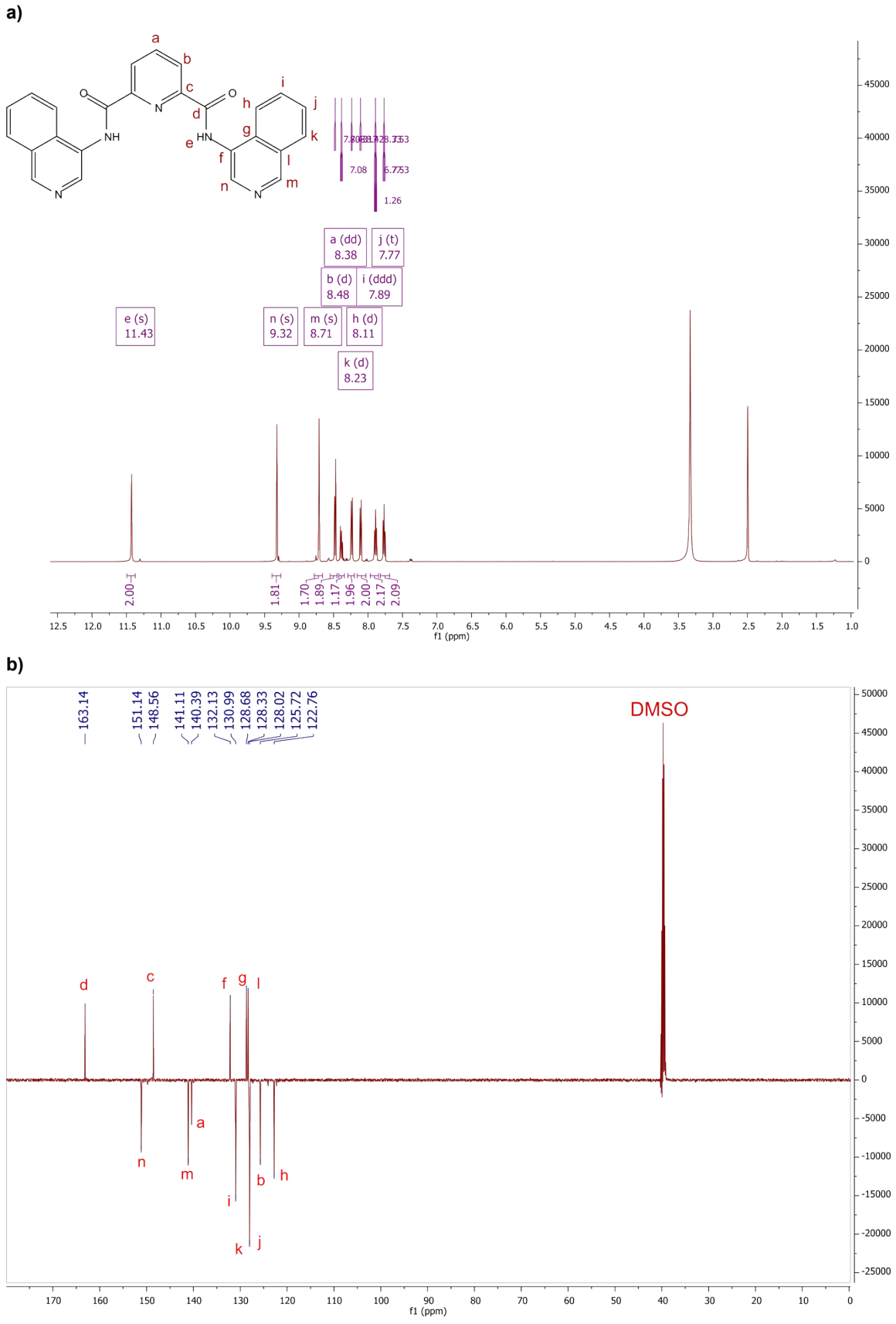

Figure S7. ^{1}H (a) and ^{13}C APT (Attached-Proton-Test) (b) NMR spectra of **1a** in DMSO-d_6.

a)

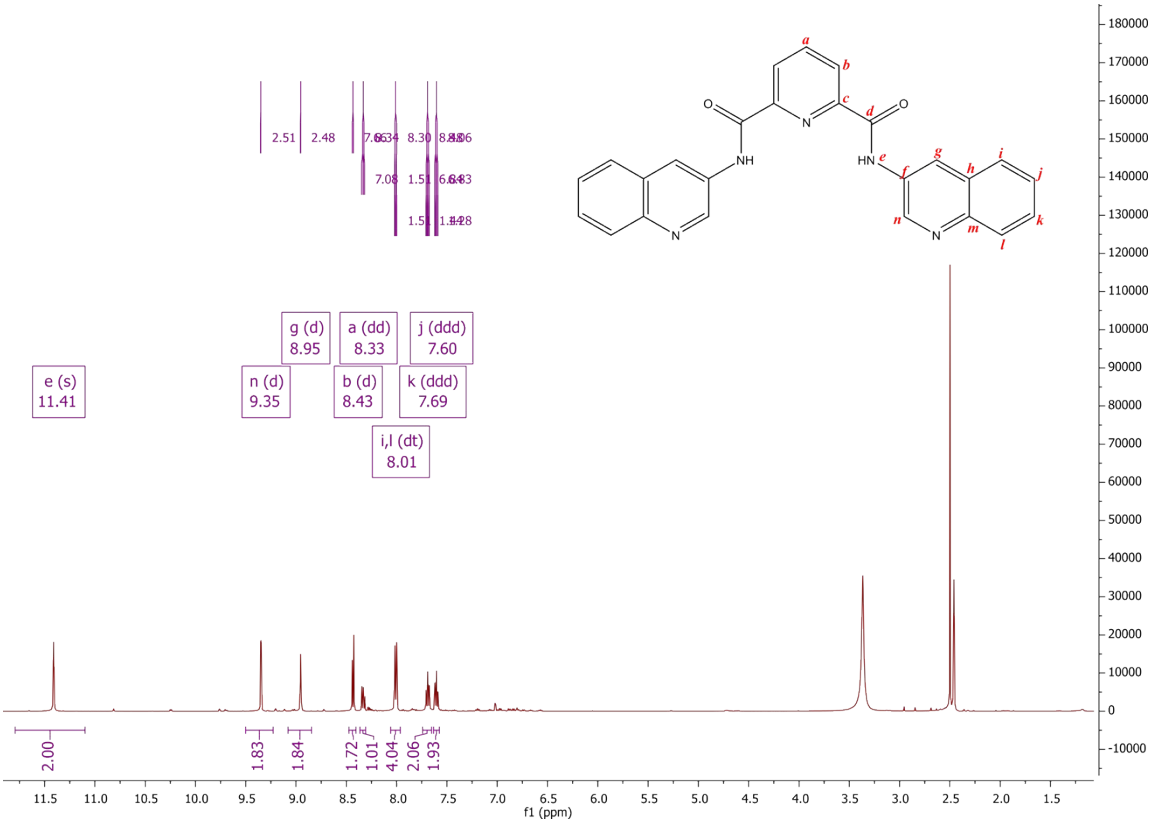

b)

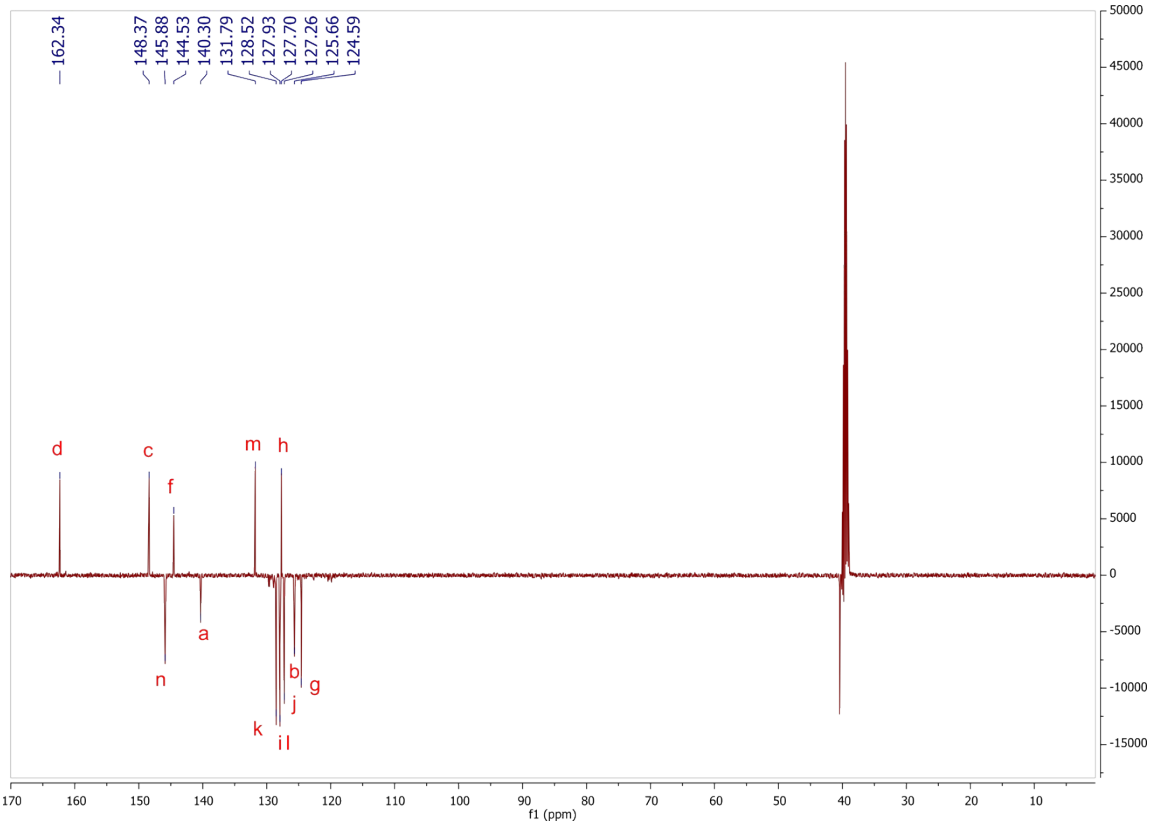

Figure S8. ^{1}H (a) and ^{13}C APT (b) NMR spectra of **1b** in DMSO-d_6.

a)

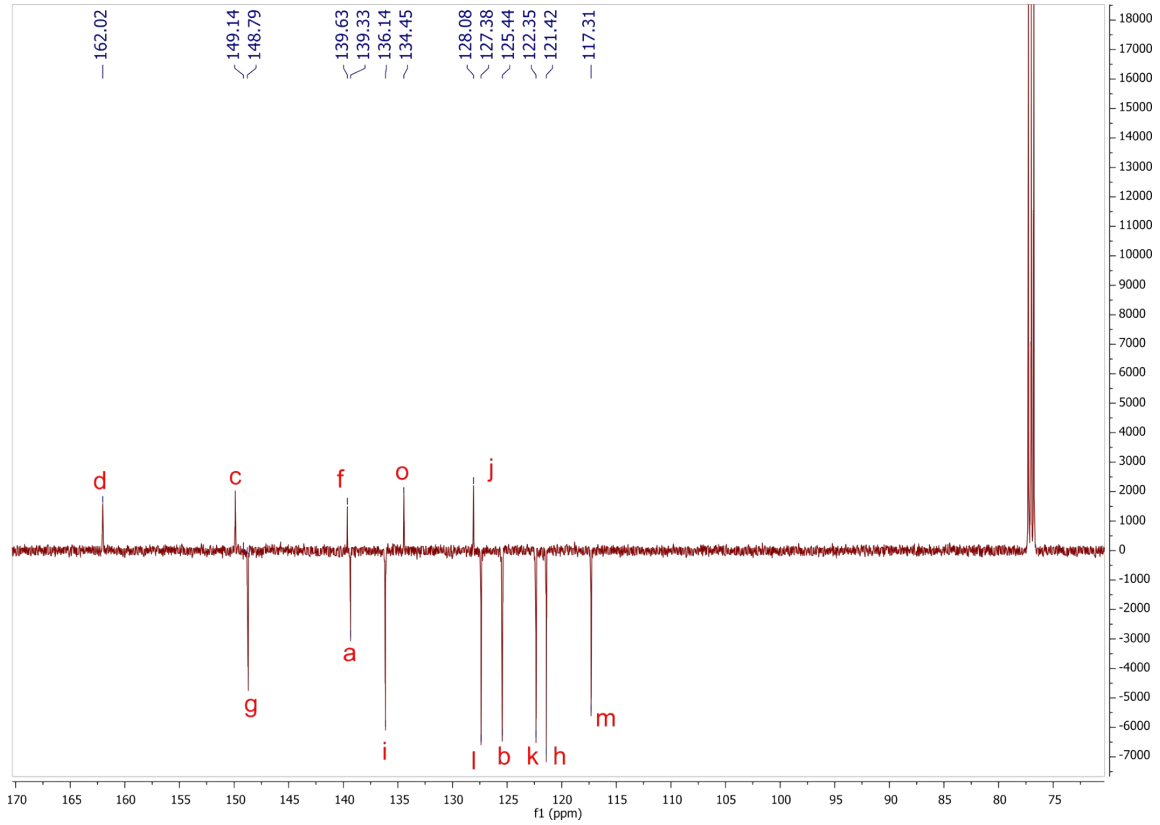

b)

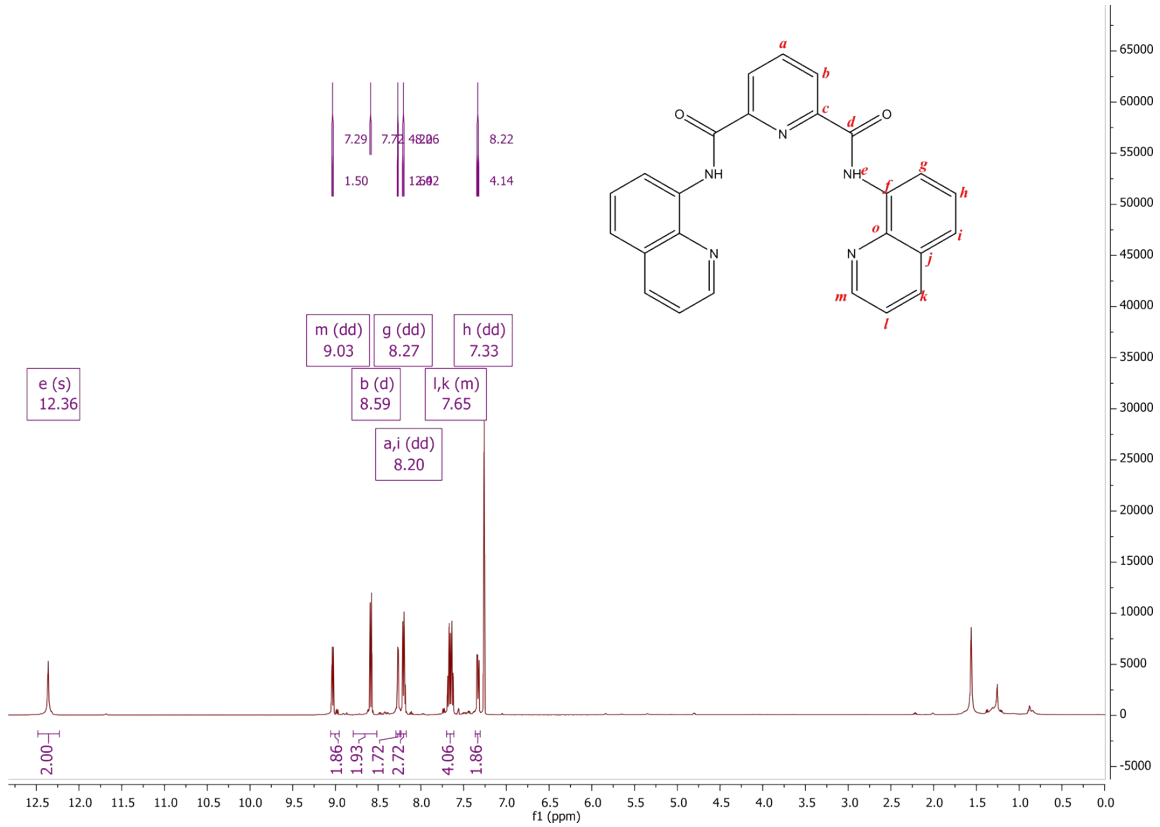

Figure S9. ^{1}H (a) and ^{13}C APT (b) NMR spectra of **1c** in DMSO-d_6.

a)

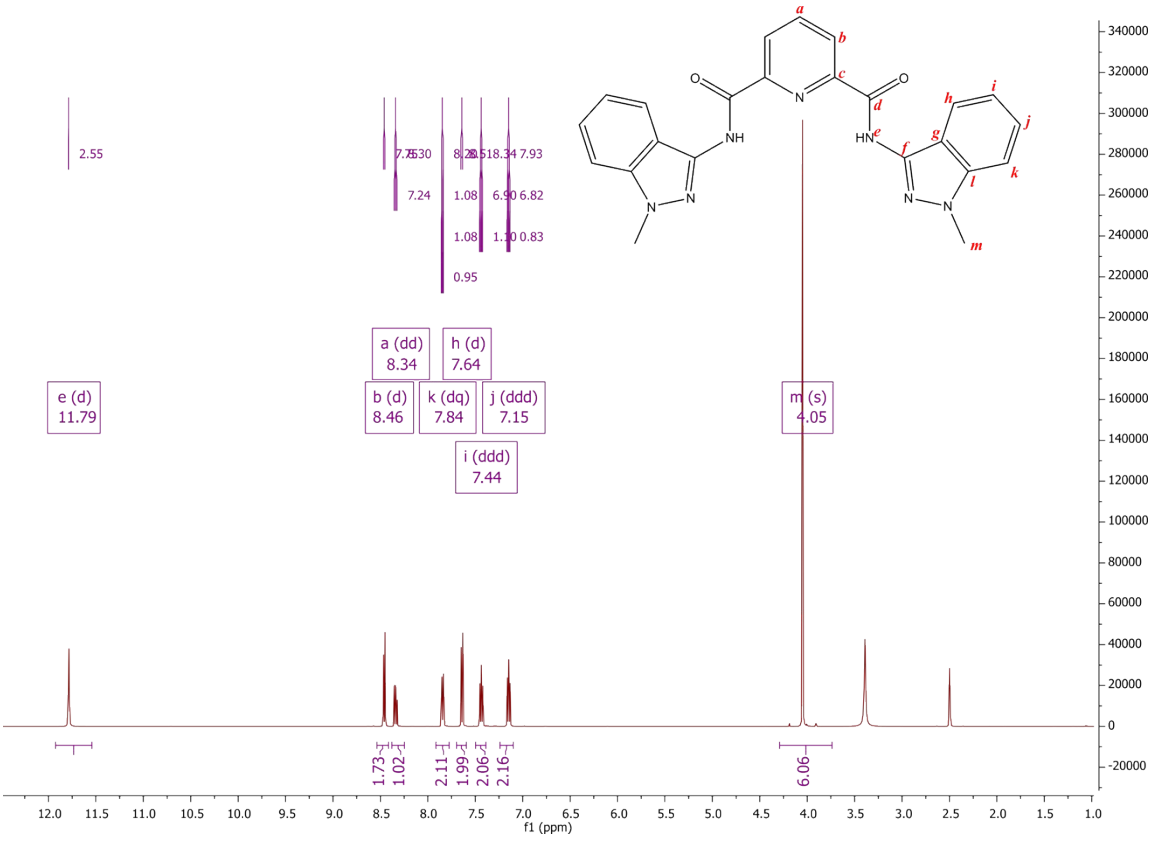

b)

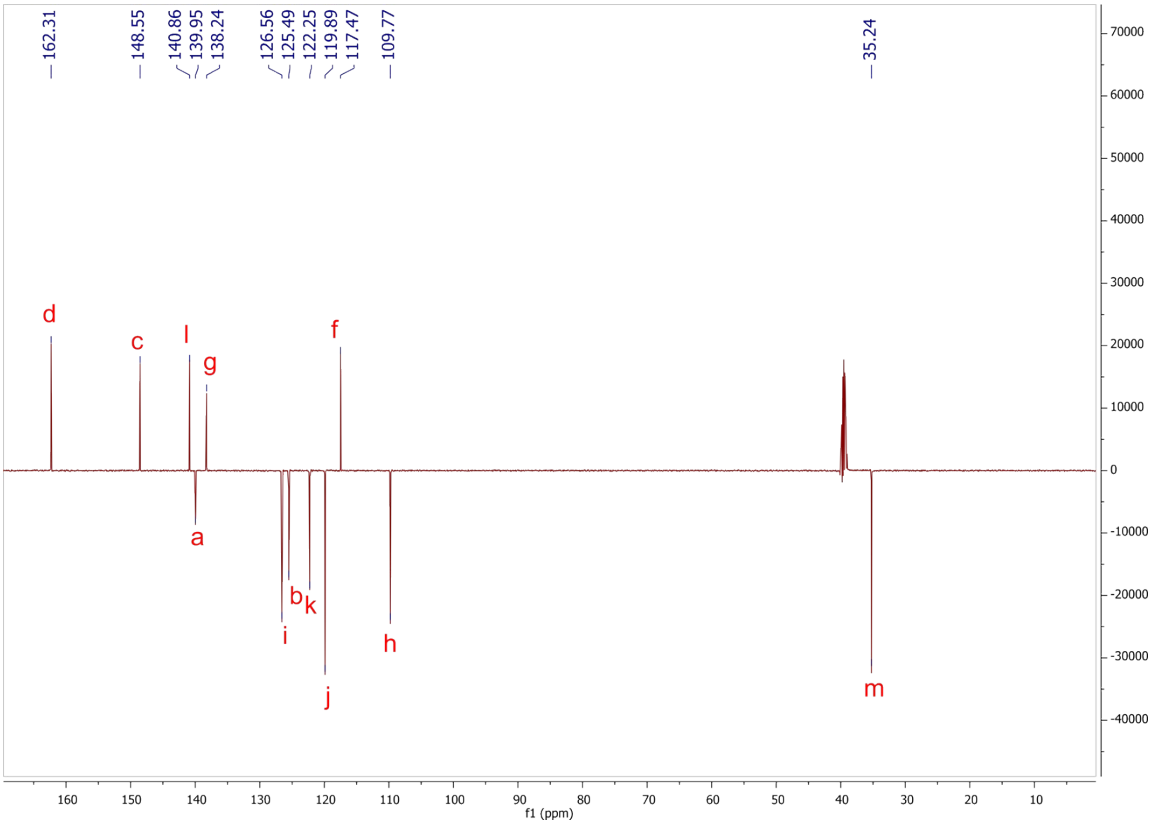

Figure S10. ^{1}H (a) and ^{13}C APT (b) NMR spectra of **1d** in DMSO-d_6.

a)

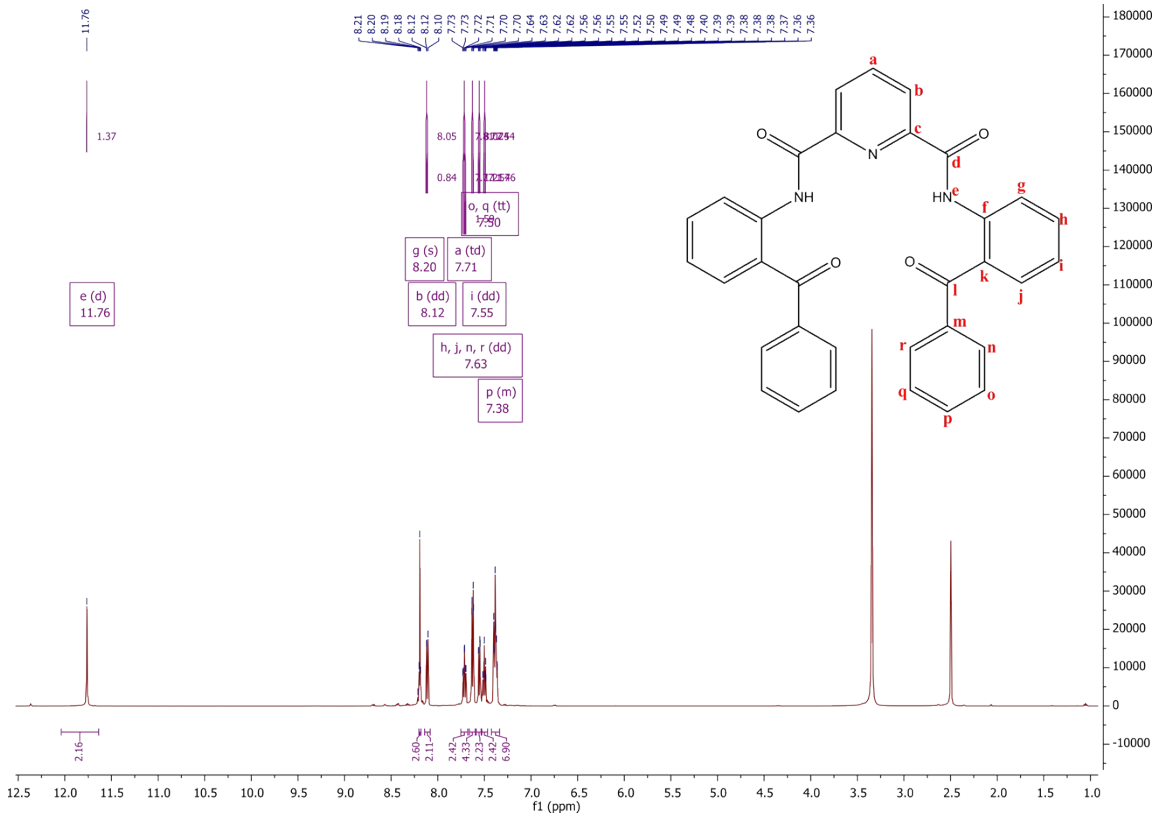

b)

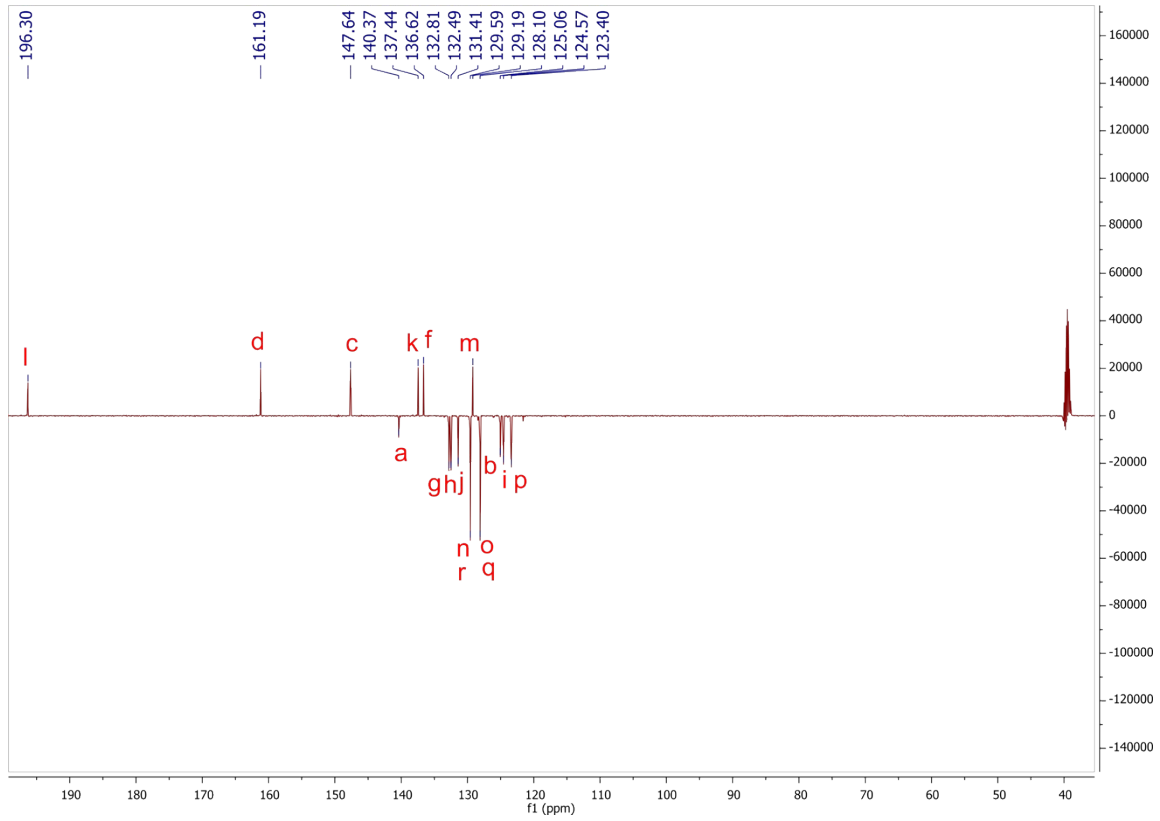

Figure S11. ^{1}H (a) and ^{13}C APT (b) NMR spectra of **1e** in MeCN-d_3.

a)

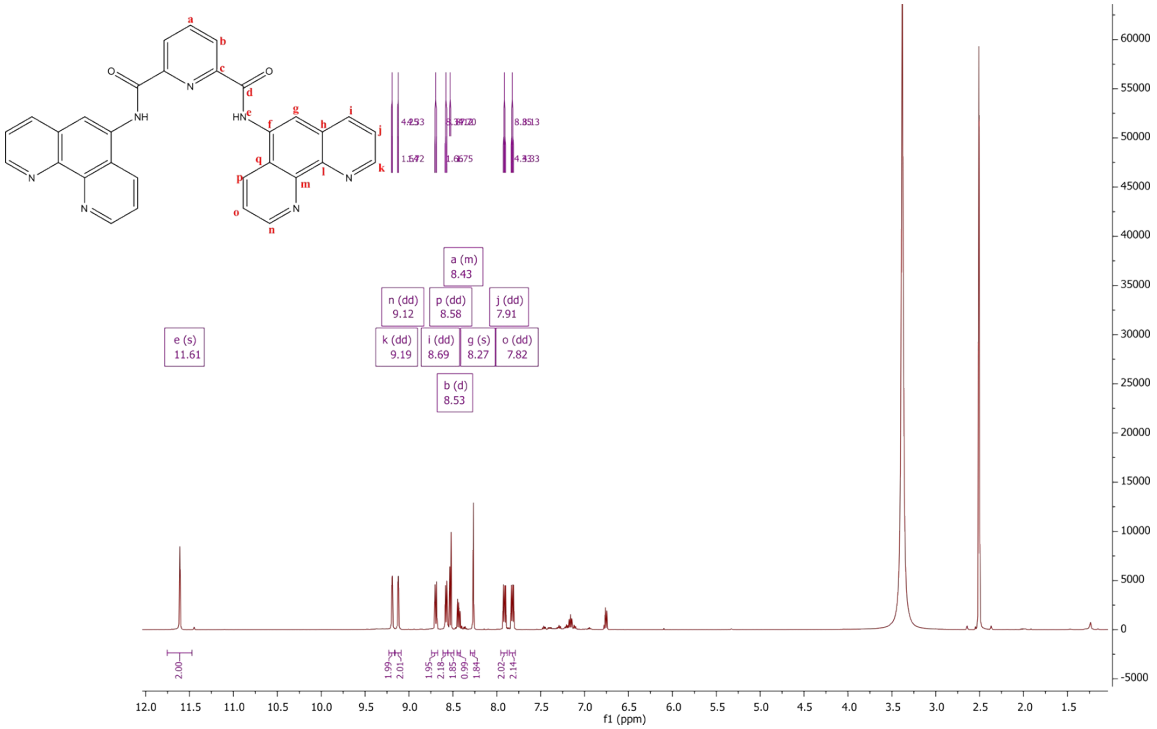

b)

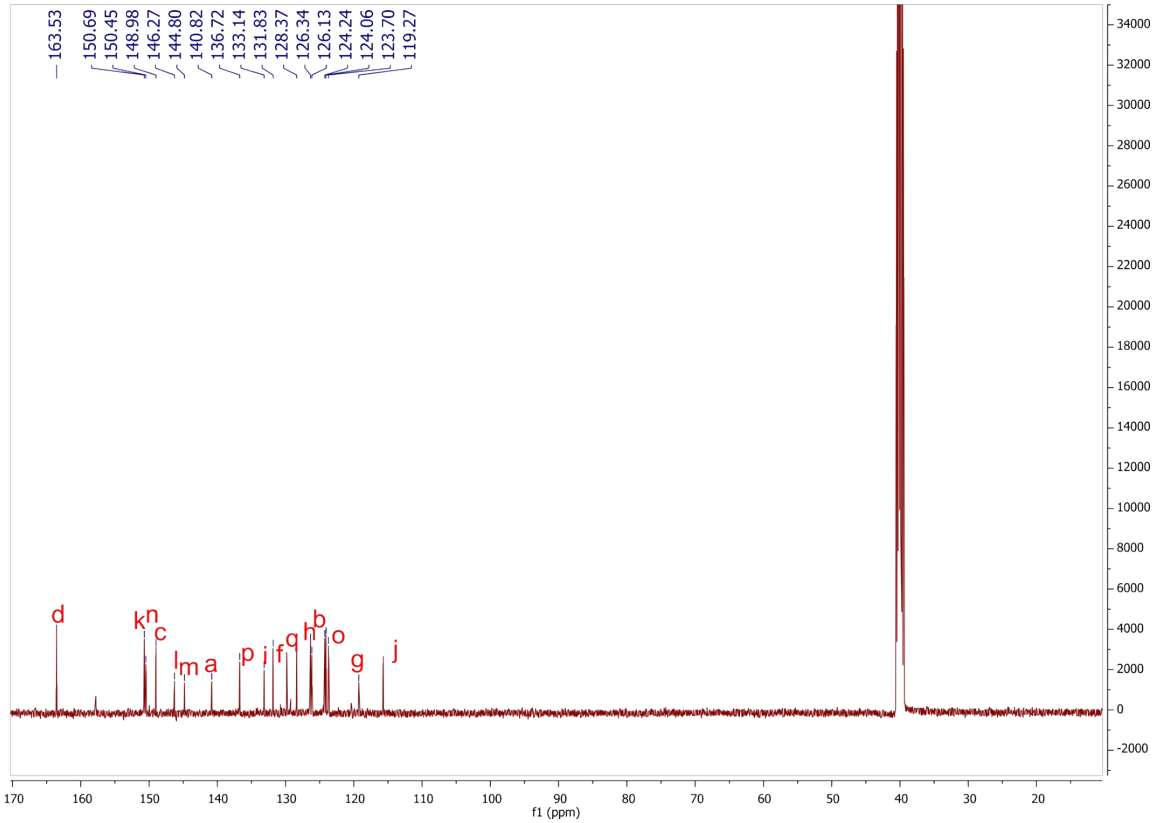

Figure S12. ^{1}H (a) and ^{13}C (b) NMR spectra of **1f** in DMSO-*d6*.

UV-vis spectroscopy

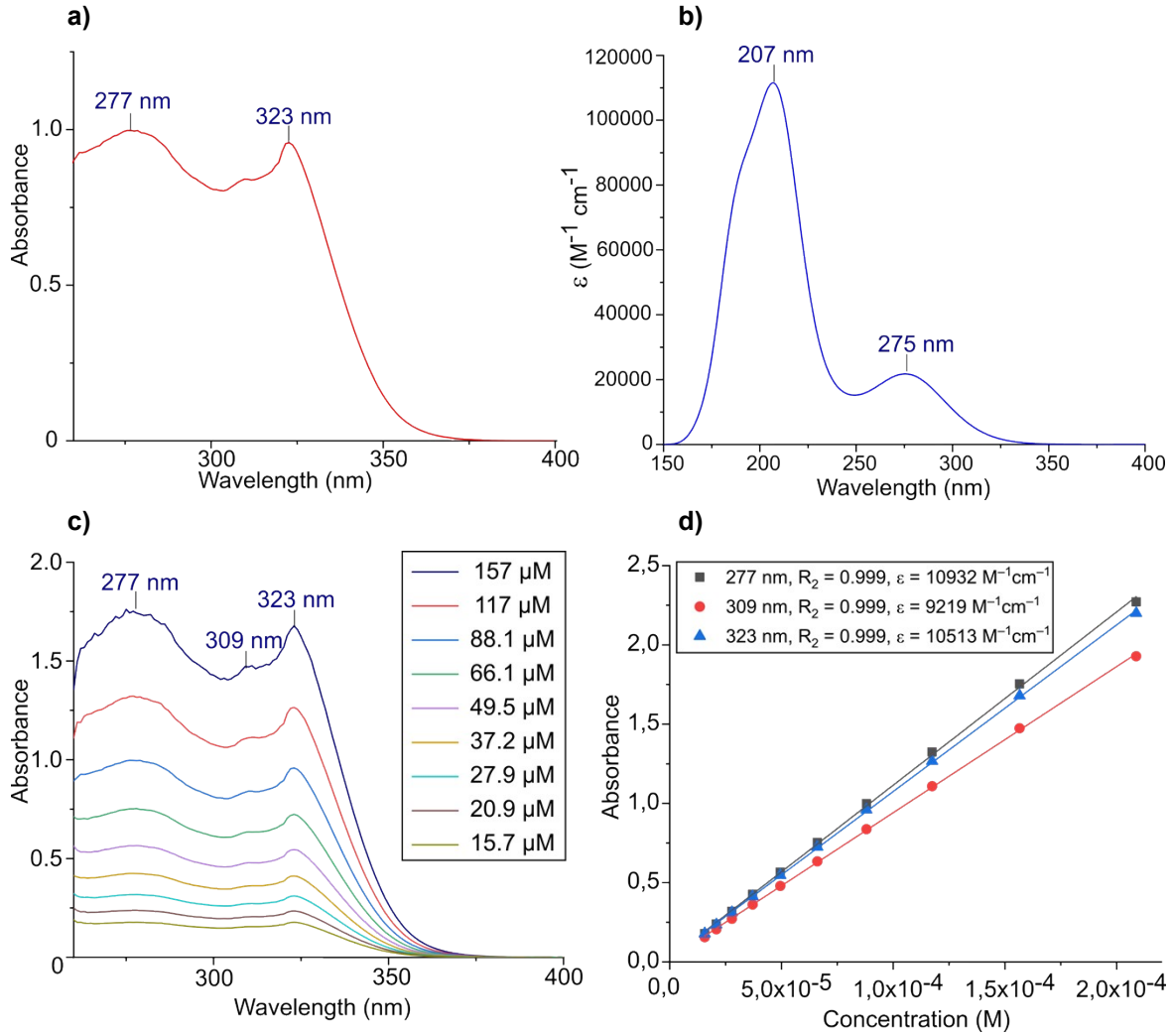

Figure S13. **(a)** Experimental and **(b)** DFT-calculated electronic absorption spectra of **1a** in DMSO. The absorption maxima are indicated for the experimental spectrum at 277, 309 and 323 nm. The absorption envelope for the DFT-calculated spectrum is plotted with a band width of 2200 cm^{-1} (full width at half maximum intensity, FWHM). **(c)** Absorption spectra at a concentration range between 16 and 157 µM, and **(d)** Linear Beer-Lambert plot (Beer-Lambert's Law),to calculate the extinction coefficients at at the λ_{max}

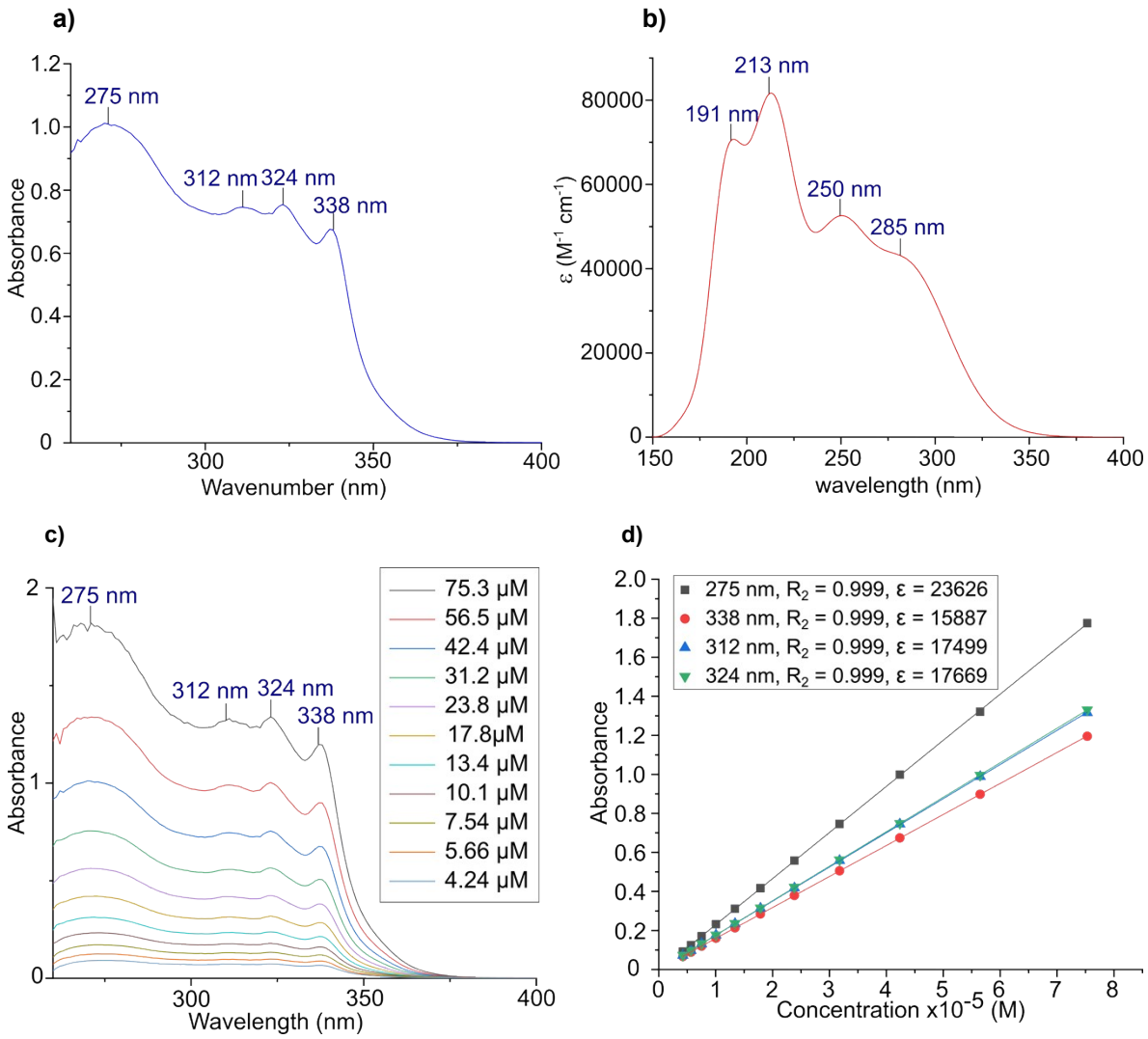

Figure S14. (a) Experimental and **(b)** DFT-calculated electronic absorption spectra of **1b** in DMSO. The absorption maxima are indicated for the experimental spectrum at 275, 312, 324 and 338 nm. The absorption envelope for the DFT-calculated spectrum is plotted with a bandwidth of 2200 cm^{-1} (full width at half maximum intensity, FWHM). **(c)** Absorption spectra at a concentration range between 4 and 75 µM, and **(d)** Linear Beer-Lambert plot (Beer-Lambert's Law),to calculate the extinction coefficients at at the λ_{max}.

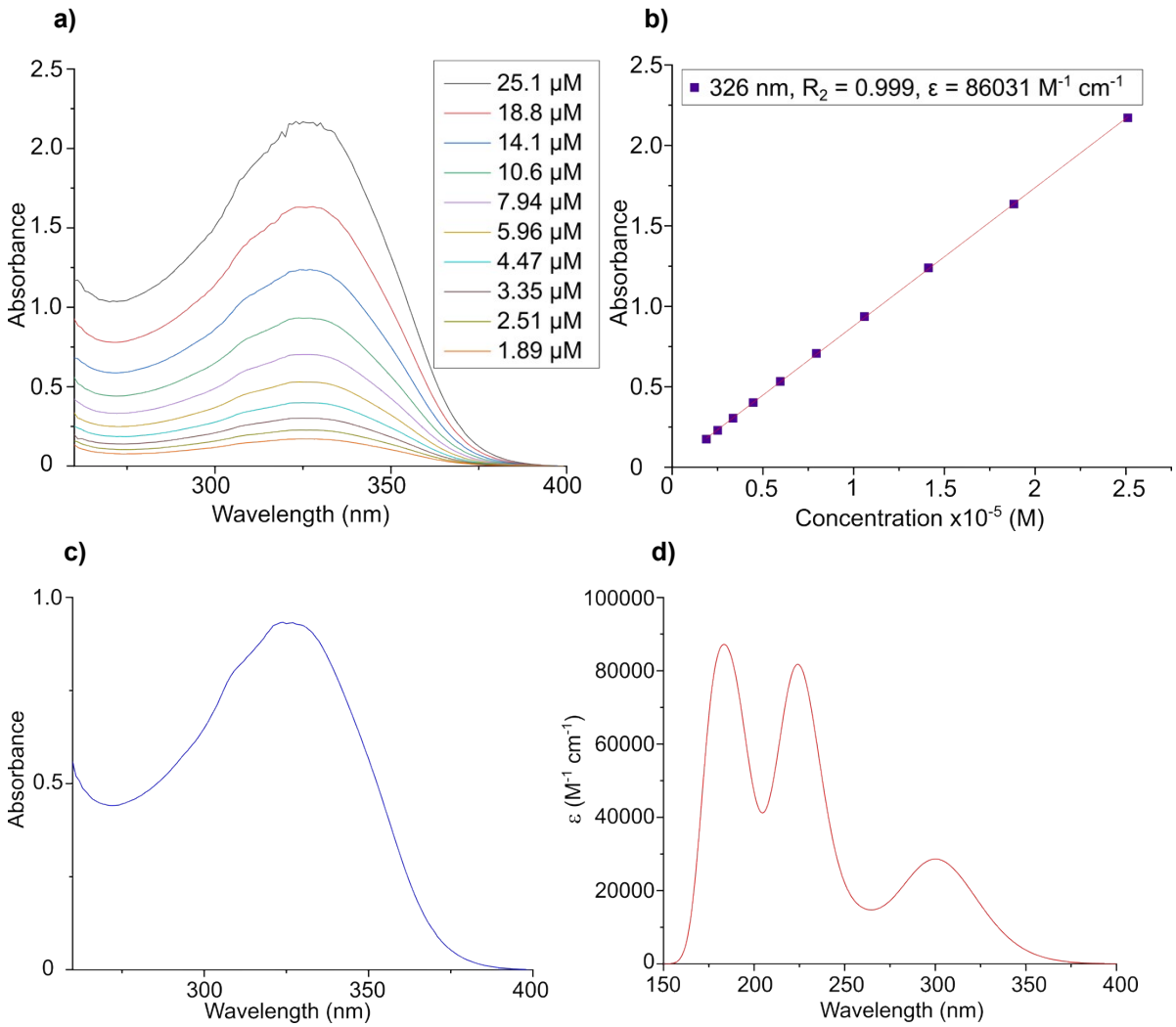

Figure S15. (a) Experimental and **(b)** DFT-calculated electronic absorption spectra of **1c** in DMSO. The absorption maxima are indicated for the experimental spectrum at 326 nm. The absorption envelope for the DFT-calculated spectrum is plotted with a bandwidth of 2200 cm^{-1} (full width at half maximum intensity, FWHM). **(c)** Absorption spectra at a concentration range between 2 and 25 μM, and **(d)** Linear Beer-Lambert plot (Beer-Lambert's Law),to calculate the extinction coefficients at at the λ_{max}.

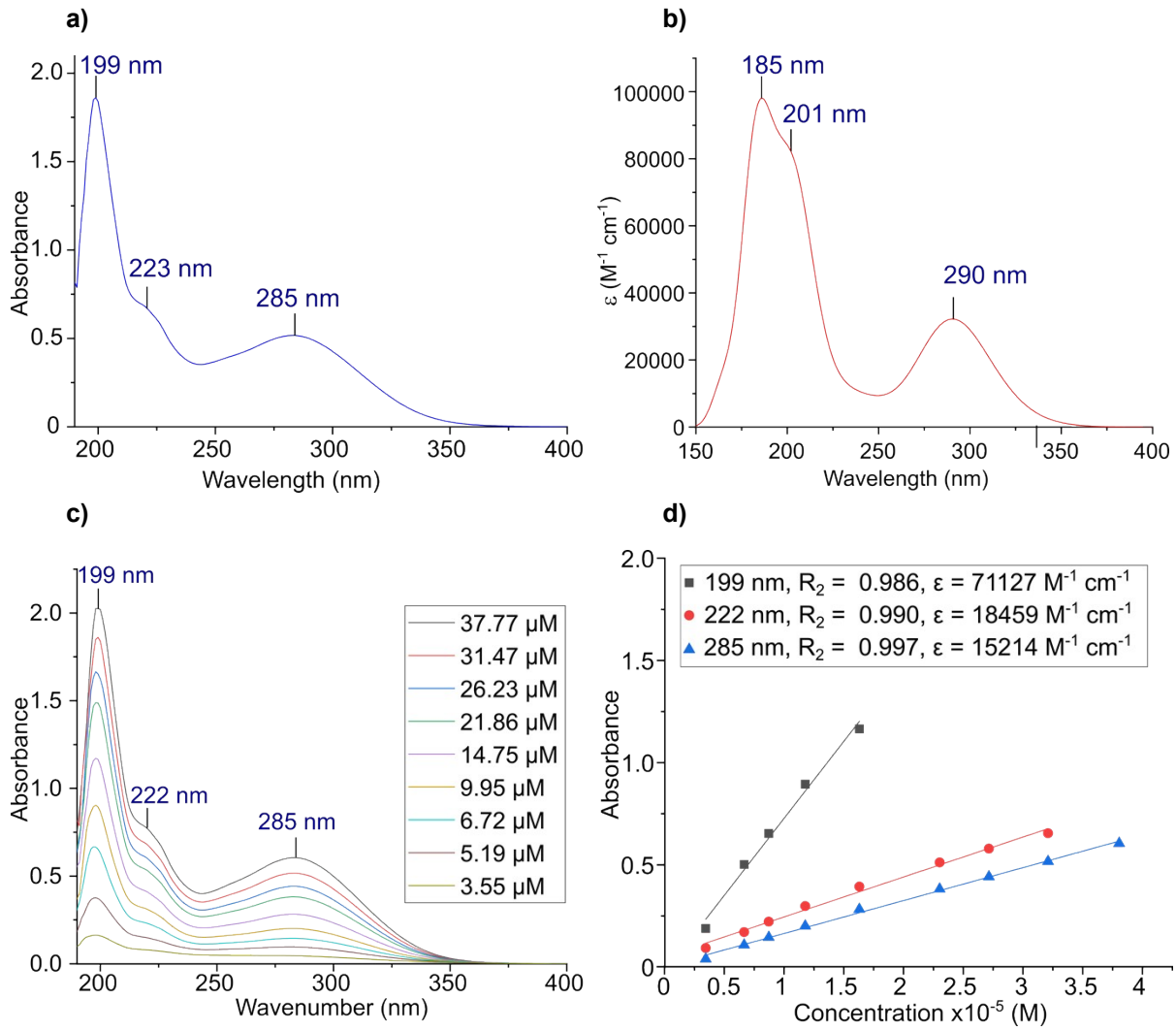

Figure S16. (a) Experimental and **(b)** DFT-calculated electronic absorption spectra of **1d** in ACN. The absorption maxima are indicated for the experimental spectrum at 199, 223, 285 nm. The absorption envelope for the DFT-calculated spectrum is plotted with a bandwidth of 2200 cm^{-1} (full width at half maximum intensity, FWHM). **(c)** Absorption spectra at a concentration range between 4 and 38 µM, and **(d)** Linear Beer-Lambert plot (Beer-Lambert's Law),to calculate the extinction coefficients at at the λ_{max}.

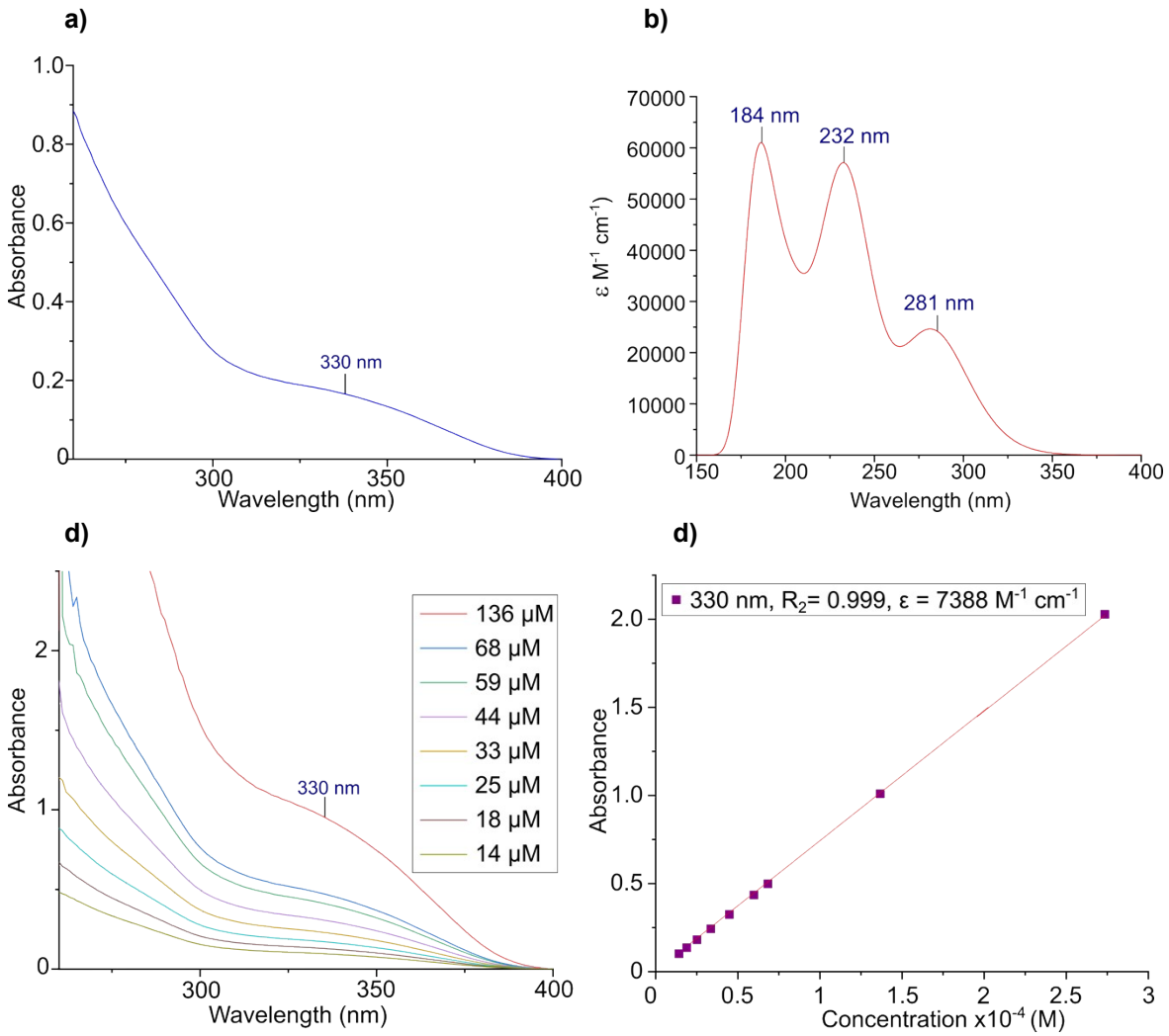

Figure S17 (a) Experimental and **(b)** DFT-calculated electronic absorption spectra of **1e** in DMSO. The absorption maxima are indicated for the experimental spectrum at 330 nm. The absorption envelope for the DFT-calculated spectrum is plotted with a bandwidth of 2200 cm^{-1} (full width at half maximum intensity, FWHM). **(c)** Absorption spectra at a concentration range between 14 and 136 μM, and **(d)** Linear Beer-Lambert plot (Beer-Lambert's Law),to calculate the extinction coefficients at at the λ_{max}.

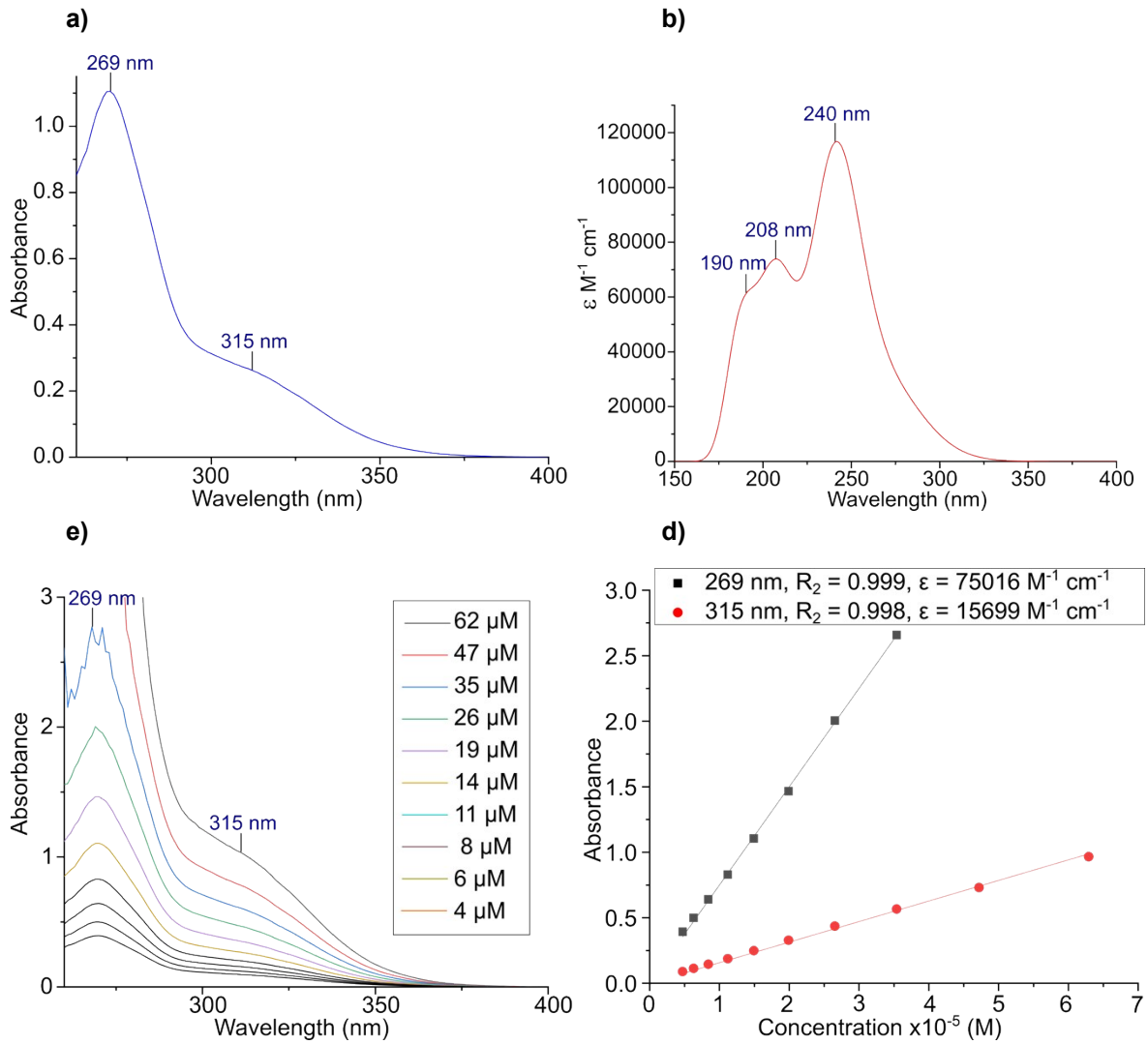

Figure S18. (a) Experimental and **(b)** DFT-calculated electronic absorption spectra of **1f** in DMSO. The absorption maxima are indicated for the experimental spectrum at 269 and 315 nm. The absorption envelope for the DFT-calculated spectrum is plotted with a bandwidth of 2200 cm^{-1} (full width at half maximum intensity, FWHM). **(c)** Absorption spectra at a concentration range between 4 and 62 μM, and **(d)** Linear Beer-Lambert plot (Beer-Lambert's Law),to calculate the extinction coefficients at at the λ_{max}.

Table 1. Calculated energies for orbital levels involved in electron transition.

	1a	1b	1c	1d	1e	1f
HOMO-3	-0.26131	-0.25499	-0.26722	-0.25245	-0.25803	-0.25291
HOMO-2	-0.26052	-0.25494	-0.26520	-0.25198	-0.25551	-0.25287
HOMO-1	-0.22929	-0.23079	-0.22469	-0.21323	-0.23921	-0.24191
HOMO	-0.22759	-0.23079	-0.22379	-0.21190	-0.23754	-0.24092
LUMO	-0.09851	-0.09771	-0.09416	-0.09335	-0.09723	-0.09549
LUMO+1	-0.09815	-0.09720	-0.09242	-0.09136	-0.09199	-0.09421
LUMO+2	-0.07289	-0.07690	-0.07370	-0.05764	-0.07768	-0.08091
LUMO+3	-0.07080	-0.07457	-0.07275	-0.05730	-0.07368	-0.07950

Table 2. Difference in energy between different HOMO and LUMO energy levels in eV

Energy levels		**Energy difference (eV)**					
		1a	**1b**	**1c**	**1d**	**1e**	**1f**
HOMO	**LUMO**	-0.12908	-0.13308	-0.12963	-0.11855	-0.14031	-0.14543
	LUMO+1	-0.12944	-0.13359	-0.13137	-0.12054	-0.14555	-0.14671
	LUMO+2	-0.1547	-0.15389	-0.15009	-0.15426	-0.15986	-0.16001
	LUMO+3	-0.15679	-0.15622	-0.15104	-0.1546	-0.16386	-0.16142
HOMO-1	**LUMO**	-0.13078	-0.13308	-0.13053	-0.11988	-0.14198	-0.14642
	LUMO+1	-0.13114	-0.13359	-0.13227	-0.12187	-0.14722	-0.1477
	LUMO+2	-0.1564	-0.15389	-0.15099	-0.15559	-0.16153	-0.161
	LUMO+3	-0.15849	-0.15622	-0.15194	-0.15593	-0.16553	-0.16241
HOMO-2	**LUMO**	-0.16201	-0.15723	-0.17104	-0.15863	-0.15828	-0.15738
	LUMO+1	-0.16237	-0.15774	-0.17278	-0.16062	-0.16352	-0.15866
	LUMO+2	-0.18763	-0.17804	-0.1915	-0.19434	-0.17783	-0.17196
	LUMO+3	-0.18972	-0.18037	-0.19245	-0.19468	-0.18183	-0.17337
HOMO-3	**LUMO**	-0.1628	-0.15728	-0.17306	-0.1591	-0.1608	-0.15742
	LUMO+1	-0.16316	-0.15779	-0.1748	-0.16109	-0.16604	-0.1587
	LUMO+2	-0.18842	-0.17809	-0.19352	-0.19481	-0.18035	-0.172
	LUMO+3	-0.19051	-0.18042	-0.19447	-0.19515	-0.18435	-0.17341

Mass spectroscopy

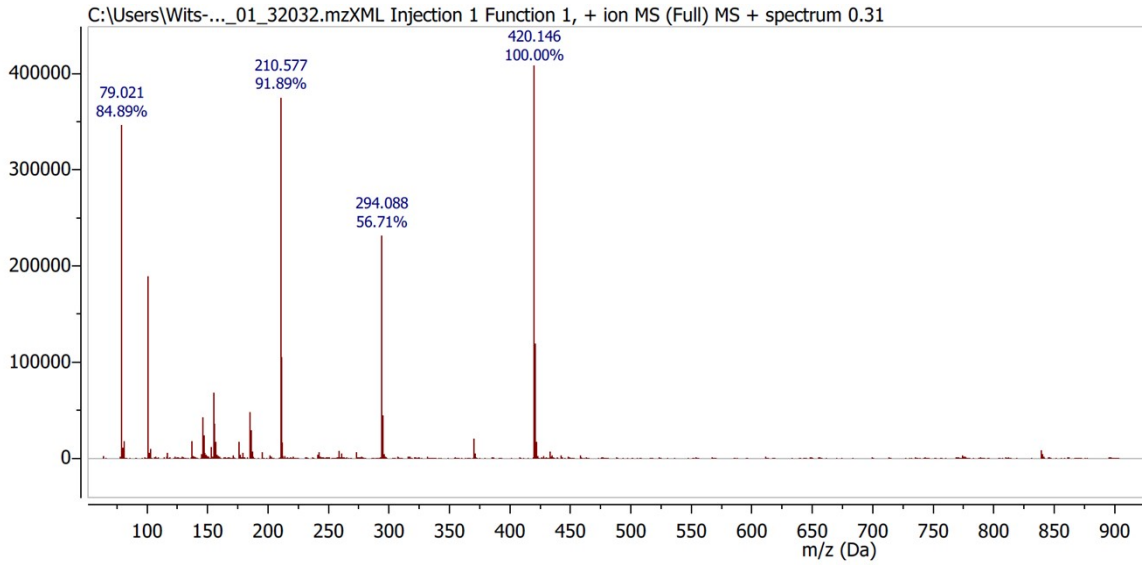

Figure S19. ESI-MS spectrum of **1a** for $C_{23}H_{18}N_5O_2$ $[M+H]^+$= 420.416. The solid sample was dissolved in ACN (1 % DMSO) with 0.1% formic acid (v/v) and the spectrum was recorded in positive ESI mode.

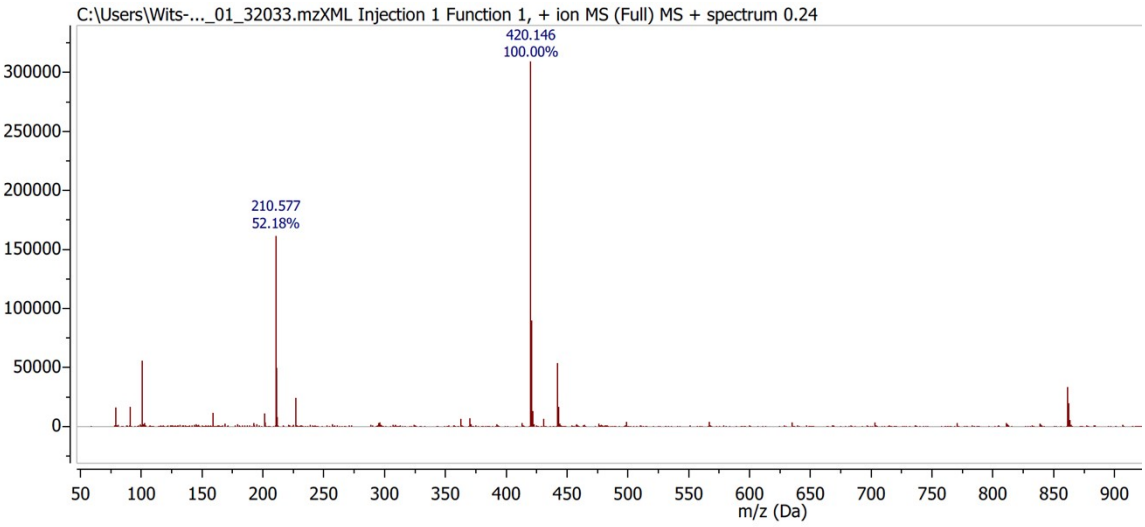

Figure S20. ESI-MS spectrum of **1b** for $C_{23}H_{18}N_5O_2$ $[M+H]^+$= 420.146. The solid sample was dissolved in ACN (1 % DMSO) with 0.1% formic acid (v/v) and the spectrum was recorded in positive ESI mode.

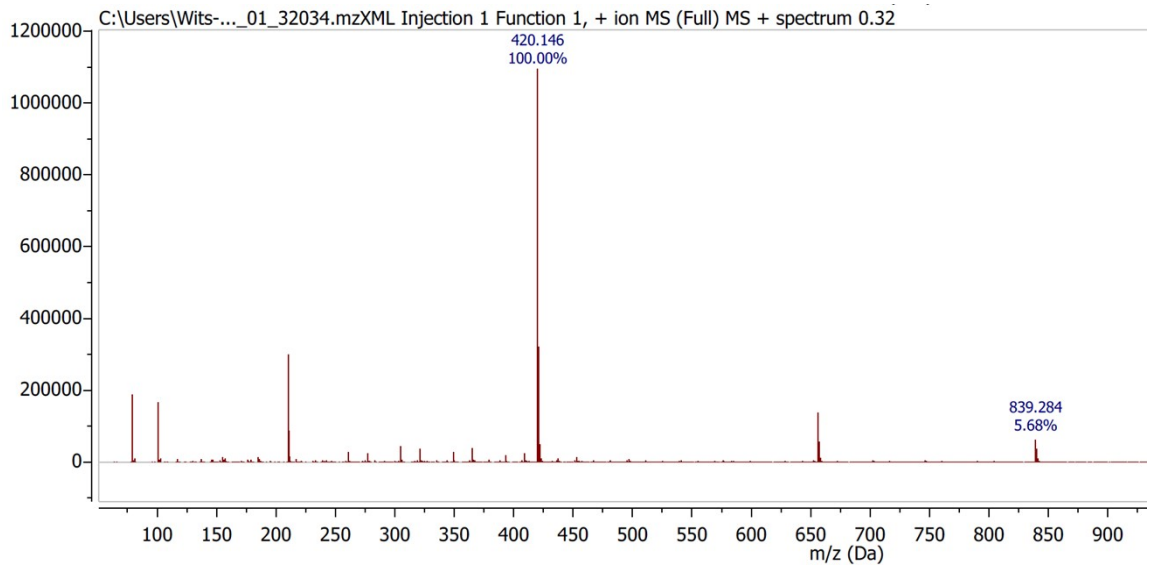

Figure S21. ESI-MS spectrum of **1c** for $C_{23}H_{18}N_5O_2$ $[M+H]^+$= 420.146. The solid sample was dissolved in ACN (1 % DMSO) with 0.1% formic acid (v/v) and the spectrum was recorded in positive ESI mode.

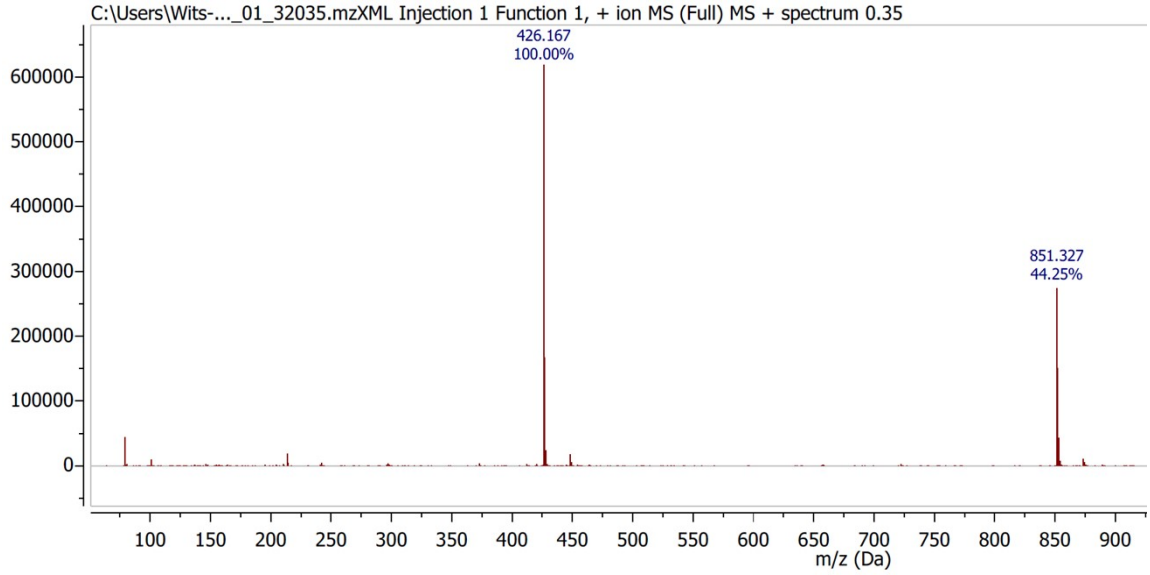

Figure S22. ESI-MS spectrum of **1d** for $C_{23}H_{18}N_5O_2$ $[M+H]^+$= 420.146. The solid sample was dissolved in ACN with 0.1% formic acid (v/v) and the spectrum was recorded in positive ESI mode.

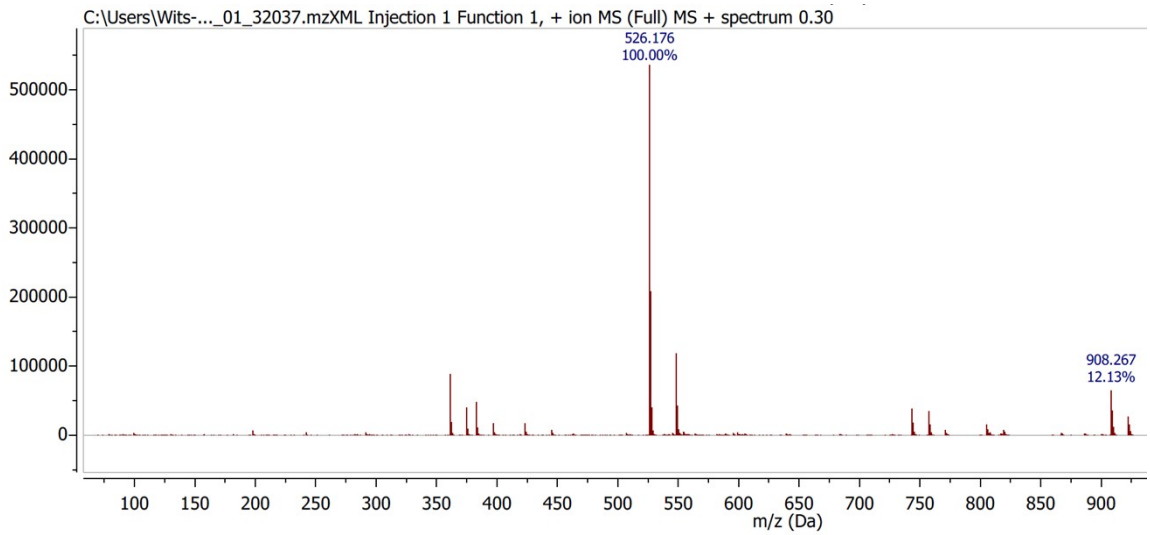

Figure S23. ESI-MS spectrum of **1e** for $C_{23}H_{18}N_5O_2$ $[M+H]^+$= 426.167. The solid sample was dissolved in ACN (1 % DMSO) with 0.1% formic acid (v/v) and the spectrum was recorded in positive ESI mode.

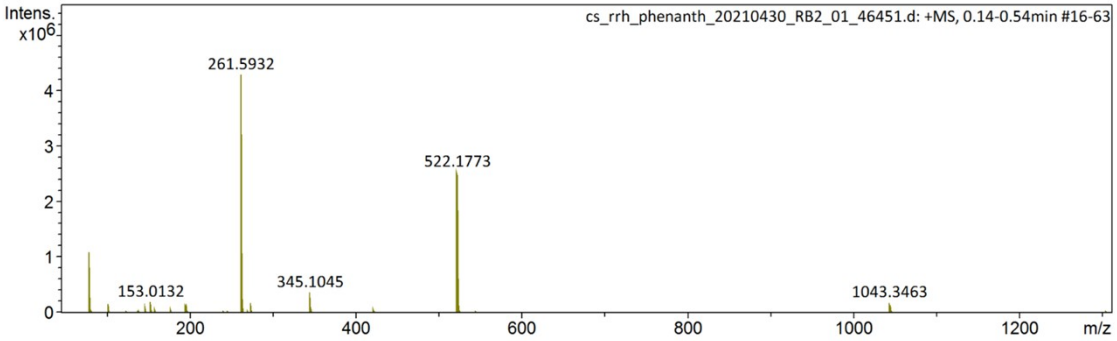

Figure S24. ESI-MS spectrum of **1f** for $C_{23}H_{18}N_5O_2$ $[M+H]^+$= 522.1773. The solid sample was dissolved in methanol with 0.1% formic acid (v/v) and the spectrum was recorded in positive ESI mode.

Xray crystallography

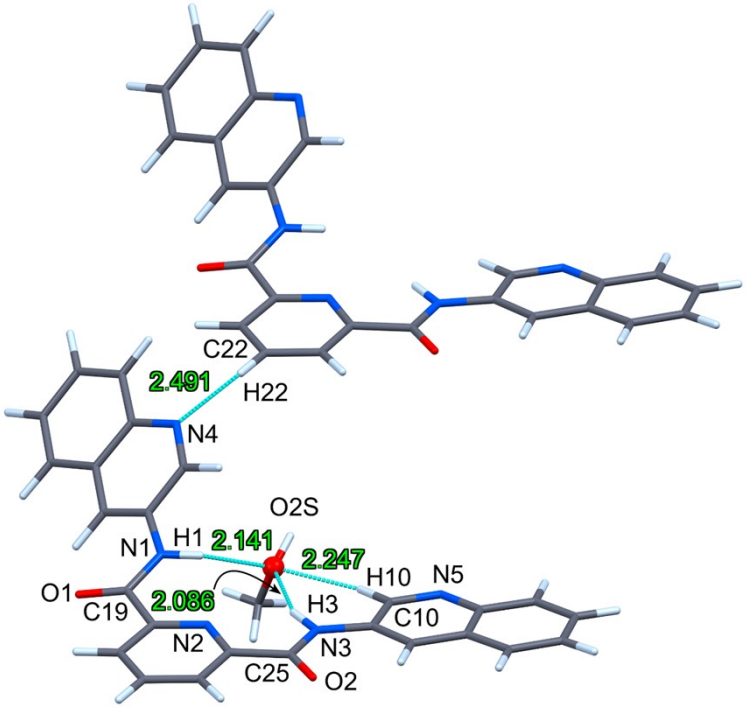

Figure S25. View of a pair of neighboring molecules in the crystal lattice of **1b**. The non-classical hydrogen bond C22–H22···N4 (2.491(7) Å) tips the quinoline ring out of the mean plane encompassing the central pyridine ring of the pincer, with the dihedral angle C19–N1–C2–C1 measuring 162.87(5)°. The dihedral angle for the second quinoline group (C25–N3–C11–C10, 176.31(5)°) is almost coplanar with the amide group and central pyridine ring.

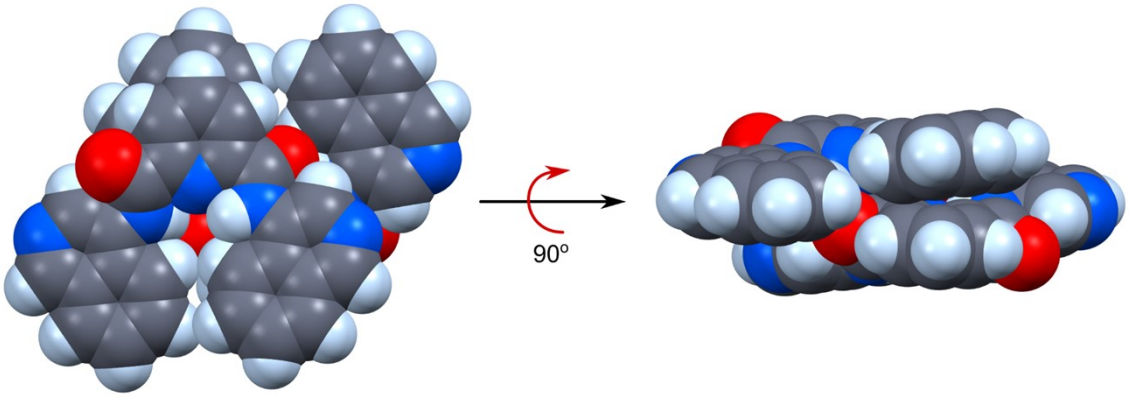

Figure S26. Space filling views of the hydrogen-bonded C_i symmetry dimer of structure **1a**. The diagram at the left is a view from above the dimer perpendicular to the plane of the pincer's central pyridine ring, while the diagram at the right is the same view rotated counterclockwise through 90° to highlight the out-of-plane arrangement of the two isoquinoline rings. The conformation of each monomer in the crystalline solid state is markedly different from the lowest-energy conformer in the gas phase (DFT simulation), which highlights the impact of crystal packing and dimer formation on the observed conformation.

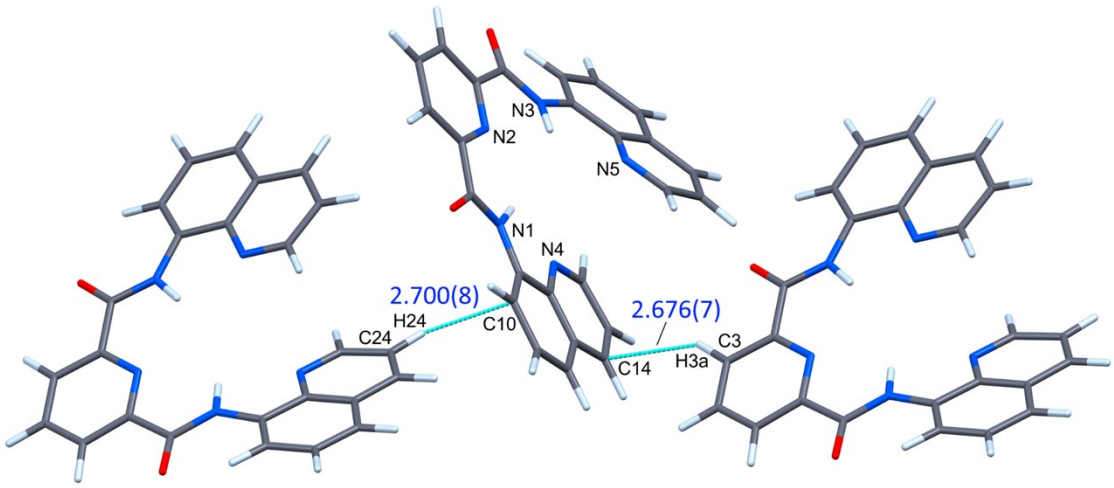

Figure S27. View depicting the short nonbonded interactions (blue stippled bonds) between the lower quinoline ring of **1c** and neighboring molecule heteroaromatic rings (contact distances are given in Å). The highlighted contacts constitute C–H···π type hydrogen bonding interactions which planarise the amide group (N1) and quinoline substituent by neatly sandwiching the substituent group. The quinoline ring appended to the second amide nitrogen atom (N5) lacks short contacts involving its aryl ring carbon atoms and thus has a more canted dihedral angle relative to the plane of the central pyridine ring of the pincer.